



Originally published as:

Cattania, C., Hainzl, S., Wang, L., Enescu, B., Roth, F. (2015): Aftershock triggering by postseismic stresses: A study based on Coulomb rate-and-state models. - *Journal of Geophysical Research*, 120, 4, p. 2388-2407.

DOI: <http://doi.org/10.1002/2014JB011500>

RESEARCH ARTICLE

10.1002/2014JB011500

Key Points:

- Inclusion of secondary triggering improves the performance of aftershock models
- Effect of afterslip on near-fault aftershocks is hard to assess due to uncertainties
- After megathrust earthquakes, afterslip enhances seismicity on crustal faults

Supporting Information:

- Readme

Correspondence to:

C. Cattania,
camcat@gfz-potsdam.de

Citation:

Cattania, C., S. Hainzl, L. Wang, B. Enescu, and F. Roth (2015), Aftershock triggering by postseismic stresses: A study based on Coulomb rate-and-state models, *J. Geophys. Res. Solid Earth*, 120, 2388–2407, doi:10.1002/2014JB011500.

Received 28 JUL 2014

Accepted 11 FEB 2015

Accepted article online 17 FEB 2015

Published online 6 APR 2015

Aftershock triggering by postseismic stresses: A study based on Coulomb rate-and-state models

Camilla Cattania¹, Sebastian Hainzl¹, Lifeng Wang², Bogdan Enescu^{3,4}, and Frank Roth¹

¹GFZ German Research Centre for Geosciences, Potsdam, Germany, ²China Earthquake Networks Center, Beijing, China, ³Earth Evolution Sciences Department, Faculty of Life and Environmental Sciences, University of Tsukuba, Tsukuba, Japan, ⁴Institute of Statistical Mathematics, Tokyo, Japan

Abstract The spatiotemporal clustering of earthquakes is a feature of medium- and short-term seismicity, indicating that earthquakes interact. However, controversy exists about the physical mechanism behind aftershock triggering: static stress transfer and reloading by postseismic processes have been proposed as explanations. In this work, we use a Coulomb rate-and-state model to study the role of coseismic and postseismic stress changes on aftershocks and focus on two processes: creep on the main shock fault plane (afterslip) and secondary aftershock triggering by previous aftershocks. We model the seismic response to Coulomb stress changes using the Dieterich constitutive law and focus on two events: the Parkfield, $M_w=6.0$, and the Tohoku, $M_w=9.0$, earthquakes. We find that modeling secondary triggering systematically improves the maximum log likelihood fit of the sequences. The effect of afterslip is more subtle and difficult to assess for near-fault events, where model errors are largest. More robust conclusions can be drawn for off-fault aftershocks: following the Tohoku earthquake, afterslip promotes shallow crustal seismicity in the Fukushima region. Simple geometrical considerations indicate that afterslip-induced stress changes may have been significant on trench parallel crustal fault systems following several of the largest recorded subduction earthquakes. Moreover, the time dependence of afterslip strongly enhances its triggering potential: seismicity triggered by an instantaneous stress change decays more quickly than seismicity triggered by gradual loading, and as a result we find afterslip to be particularly important between few weeks and few months after the main shock.

1. Introduction

The crust responds to a large earthquake with a variety of seismic and aseismic phenomena, including aftershock sequences, aseismic slip concentrated along the plate interface (afterslip), viscoelastic relaxation distributed in the asthenosphere [K. Wang *et al.*, 2012], and displacement of fluids giving rise to poroelastic rebound [Nur and Booker, 1972; Cocco and Rice, 2002]. These processes are induced by local changes in the stress field, and they in turn cause stress redistribution: physics-based models aimed at describing aftershock sequences should consider the interplay of these phenomena.

1.1. Afterslip

Afterslip is a widespread postseismic process [Marone *et al.*, 1991], and it is considered the most significant source of surface displacement in the first few hundred days following the main shock, while viscoelastic relaxation becomes increasingly significant at later times [K. Wang *et al.*, 2012; Diao *et al.*, 2014]. Several authors have suggested that afterslip plays a central role in triggering aftershocks [Benioff, 1951; Schaff *et al.*, 1998; Perfettini, 2004; Savage *et al.*, 2007; Helmstetter and Shaw, 2009; Gualandi *et al.*, 2014]: the total moment release of afterslip can be comparable to the coseismic moment [Pritchard and Simons, 2006], and it generates similar static stress changes as the main shock.

Perfettini [2004] suggests that aseismic creep in the brittle creep fault zone (downdip of the coseismic rupture) is responsible for triggering aftershocks; this model, which assumes a linear dependence between slip rate and aftershock rate, is in agreement with the mechanism suggested by Schaff *et al.* [1998] to explain the interevent time of repeating earthquakes. On the other hand, the assumption of linearity between slip rate and seismicity rate has been questioned (for example, by Hsu *et al.* [2007], Savage [2010], and Helmstetter and Shaw [2009]). In the rate-and-state formulation, a power law decay arises from the nucleation time of a population of velocity weakening patches: the finite nucleation time introduces a delay

following an instantaneous stress step so that time-dependent stresses are no longer required to explain the temporal evolution of seismicity.

1.2. Secondary Triggering

Another source of postseismic stresses are the aftershocks themselves. The seismic moment released by aftershocks is typically a small fraction of the coseismic moment [e.g., *Zakharova et al.*, 2013] and of the afterslip moment [*Perfettini*, 2004]; for this reason, only the largest or the few largest events are normally considered in Coulomb studies. On the other hand, *Meier et al.* [2014] showed that about a third of the aftershocks following the Landers main shock experienced larger stress changes from aftershocks than from the main shock. This finding is in agreement with *Marsan* [2005], who showed that given a fractal distribution of hypocenter locations and a Gutenberg-Richter distribution of magnitudes, small events can be as effective as large ones at generating stress perturbations.

All these lines of evidence indicate that both afterslip and secondary triggering play an important role in triggering aftershocks. On the other hand, a gap exists between these observations and physics-based models of aftershocks sequences developed in an operational forecasting context: with few exceptions [e.g., *Strader and Jackson*, 2014], these models do not usually include information about postseismic stresses [*Hainzl et al.*, 2010]. In this study, we use aftershock models based on Coulomb stress transfer and rate-and-state friction (henceforth referred to as CRS models) to quantify the role of afterslip and secondary triggering in generating aftershocks. We focus on two case studies from different tectonic settings, both characterized by intense geodetic and seismic monitoring: the 2004 Parkfield ($M_w = 6.0$) and the 2011 Tohoku ($M_w = 9.0$) earthquakes. We use a statistical measure of model performance (information gain) to verify whether the inclusion of postseismic processes improves the spatiotemporal fit to the observed aftershocks.

After outlining the modeling framework (section 2), we present a comparison of CRS models, and we assess the general effect of postseismic stresses. In section 4, we discuss several factors controlling model behavior. In particular, we assess the importance of the location and the temporal evolution of afterslip in triggering aftershocks, and we discuss the implications of these results in a global perspective. Our goal is twofold: on one hand, we aim to gain physical insight into the relative role of coseismic and postseismic stresses in triggering aftershocks and on the other hand, we test whether the inclusion of afterslip and aftershocks has the potential to improve operational earthquake forecasts aimed at modeling seismicity in the few hundred days following a large event.

2. Methods

2.1. Coulomb Stresses

According to the Mohr-Coulomb failure criterion, sliding along a fault occurs when the shear stress exceeds the frictional strength, which is linearly related to the normal stress: this implies that a fault can be brought closer to failure by an increase in shear stress or by a decrease in normal pressure. Coulomb stress changes are defined as

$$\Delta\text{CFS} = \Delta\tau - \mu\Delta\sigma_{\text{eff}} \quad (1)$$

where τ is the shear stress, μ is the coefficient of friction, and $\sigma_{\text{eff}} = \sigma - p$ is the effective normal stress, with σ the loading stress and p the pore pressure; shear and normal stresses are calculated by resolving the stress tensor on a given fault plane (receiver fault). The Coulomb stress hypothesis states that seismicity can be triggered where $\Delta\text{CFS} > 0$, and inhibited where $\Delta\text{CFS} < 0$.

2.2. Rate-and-State Seismicity Evolution

While the Coulomb stress hypothesis has had some success in predicting the spatial distribution of aftershocks following coseismically induced static stress changes [*King et al.*, 2004], it does not account for the temporal evolution of seismicity. A common modeling approach consists of coupling Coulomb stress calculations with the constitutive law for the evolution of seismicity derived by *Dieterich* [1994]. By considering stress perturbations on an infinite population of faults governed by rate-and-state (RS) friction, seismicity rate is shown to evolve as follows:

$$R = \frac{r_0}{\dot{\gamma}} \quad (2)$$

$$d\gamma = \frac{1}{A\sigma} [dt - \gamma dS] \quad (3)$$

where γ is the seismicity state variable, r_0 is the background seismicity rate, $\dot{\tau}$ the secular stressing rate, t is time, A a constitutive parameter, and $S = \tau - (\mu - \alpha)\sigma_{\text{eff}}$, with α a positive nondimensional parameter [Linker and Dieterich, 1992]. Since μ and α are constants, ΔS can be identified with ΔCFS (equation (1)) with $\mu \rightarrow \mu - \alpha$. Pore pressure changes can be assumed to be proportional to normal pressure changes [Cocco and Rice, 2002, and references therein]: $\Delta p = -B\Delta\sigma$, with B the Skempton coefficient which varies between 0 and 1. By using a modified coefficient of friction $\mu' = (\mu - \alpha)(1 - B)$, we obtain $\Delta S = \Delta\tau - \mu'\Delta\sigma$. The choice of the parameter μ' has only a modest impact on model behavior [Cattania et al., 2014]; we use a value of 0.3.

2.3. Model Setup

Coulomb stresses are calculated on a 3-D grid, and equations (2) and (3) are solved individually for each grid point. For simplicity, the rate-and-state parameters $A\sigma$ and $t_a = A\sigma/\dot{\tau}$ and r_0 are assumed to be spatially uniform; we estimated the value for r_0 from the catalog of past seismicity and fitted $A\sigma$ and t_a to the observed aftershock sequence. Optimal parameters were found by maximizing the log likelihood [Zhuang et al., 2012]: for a model $R(\mathbf{x}, t)$ and a catalog with N events at $(\mathbf{x}_1, t_1; \mathbf{x}_2, t_2; \dots; \mathbf{x}_N, t_N)$ in the time period $[t_0, t_1]$, this is defined as

$$\text{LL} = \sum_i^N \log(R(\mathbf{x}_i, t_i)) - \int_{t_0}^{t_1} \int_{\text{volume}} R(\mathbf{x}, t) d\mathbf{x} dt \quad (4)$$

In order to restrict the parameter estimation to a time period in which the catalog is complete [Kagan, 2004], we skipped a time window following the main shock, when the completeness magnitude is above the target magnitude (see section 2.6).

Several studies [Hainzl et al., 2009; Woessner et al., 2012; Cattania et al., 2014] have shown that Coulomb stress calculations suffer from large uncertainties, the most important of which are the choice of input slip model and the unknown orientation of the receiver faults on which the stress tensor should be resolved. The latter can be considered as a source of aleatoric uncertainties, which generates spatial variations of Coulomb stress; such heterogeneity can be estimated by performing Monte Carlo simulations on a set of possible fault orientations (from the catalog of past focal planes) and adding up the seismicity rates from each fault to give an average rate. Details on this method, as well as on the estimation of the background seismicity rate and consideration of uncertainties in earthquake locations, can be found in Cattania et al. [2014].

While assuming a uniform background rate is unrealistic, this simplification allows to more easily assess the role of stress distribution in the seismicity; moreover, previous work by Cocco et al. [2010] indicates that CRS models can be very sensitive to the relative location of background rate and ΔCFS , thus amplifying uncertainties in stress calculations.

2.4. Calculating Time-Dependent Stresses and Rates

We consider static stresses generated by coseismic slip, afterslip, and aftershocks. All slip model-based calculations are obtained from the analytical solutions for rectangular dislocations in an elastic half-space [Okada, 1992].

A general, time-dependent stressing history can be modeled by approximating it by a piecewise linear function and solving equations (2) and (3) for each time step using the analytical solution for linear stressing [Dieterich, 1994]. Since afterslip might be space and time dependent, each patch may experience a different temporal evolution. However, we find that the model behavior is not changed significantly by approximating the afterslip as spatially stationary: for computational efficiency, we therefore assumed a spatially uniform temporal evolution $F(t)$. As shown by Savage [2010], the cumulative afterslip following Parkfield evolves according to

$$F(t) \propto A \log(1 + t/t_1) + B \log(1 + t/t_2) + C \log(1 + t/t_3) \quad (5)$$

with $A = 23.7$, $B = 9.02$, $C = 6.15$, $t_1 = 4.06$, $t_2 = 0.11$, and $t_3 = 10^{-4}$. For Tohoku, we found that the time series can be fit by a single logarithmic function: we obtained $A = 1$, $B = C = 0$, and $t_1 = 14.2$, in agreement with Perfettini and Avouac [2014].

To calculate the stresses imposed by aftershocks, we created a square synthetic slip model based on the focal mechanisms solutions and the empirical relations of *Wells and Coppersmith* [1994]. For most aftershocks focal mechanisms are not available: in these cases, we followed the approach of *Chen et al.* [2013] and approximated the stress field by

$$\Delta\text{CFS} = \frac{M_0}{6\pi r^3} \quad (6)$$

where M_0 is the seismic moment and r the distance to the earthquake hypocenter. We considered stress changes from all aftershocks above the magnitude of target events (described in section 2.6) from $t = 0$.

2.5. Model Tested and Performance Evaluation

To verify whether modeling postseismic stresses has the potential to improve aftershock forecasts, we compare a starting model with only coseismic stresses (Model 0) with three models accounting additionally for postseismic effects: one including time-dependent stresses from afterslip (Model 1), one including secondary triggering (Model 2), and one including both processes (Model 3). Rate-and-state parameters $A\sigma$ and t_a are inverted independently for each model.

The performance of a model is quantified by the log likelihood (equation (4)); to compare models, we used the average difference in log likelihood (information gain):

$$I = \frac{LL - LL_0}{N} \quad (7)$$

where LL is the model log likelihood, LL_0 refers to Model 0, and N the total number of aftershocks. To quantify the effect of postseismic effects on individual events, we consider the information gain of single aftershocks:

$$I_{ev} = LL_i - LL_{0,i} = \log(R(x_i, t_i)) - \log(R_0(x_i, t_i)) - \int_{t_{i-1}}^{t_i} \int_{\text{volume}} [R(\mathbf{x}, t) - R_0(\mathbf{x}, t)] \, d\mathbf{x} dt \quad (8)$$

The above quantity includes the ratios of the probability density functions of waiting times and locations given by the considered model and the reference model [Zhuang et al., 2012]. A related quantity is the ratio of probabilities between each model with respect to Model 0 (or probability gain), given by $G = \exp(I_{ev})$. This quantity has a more intuitive physical interpretation, since it is proportional to the ratio of the probabilities of individual events between models.

2.6. Data

For Parkfield, we considered the area shown in Figure 1 and a depth range between [0.5, 11.5] km. We used the independent coseismic and afterslip models of *L. Wang et al.* [2012], based on Bayesian inversion of GPS data; the earthquake catalog is a combination of the Advanced National Seismic System (ANSS) catalog (starting from 1970) and the more complete catalog of *Peng and Zhao* [2009] for the first 2 days.

The model domain for Tohoku corresponds to the area shown in Figure 2 and a depth range between [3.0, 42.0] km. We used the catalog provided by the Japan Meteorological Agency (starting from 2010) and the GPS-based slip models of *Wang et al.* [2013]. A large number of coseismic and postseismic slip models have been produced for the Tohoku earthquake, and the performance of CRS models can vary significantly between them [Cattania et al., 2014]: in order to estimate the reliability of our results, we repeated the calculations for Tohoku using the coseismic and postseismic slip models of *Perfettini and Avouac* [2014]. While the coseismic slip distribution is in broad agreement with other published slip models, the afterslip distribution is significantly different: the authors find large shallow afterslip, overlapping with the area of coseismic slip. On the other hand, the patch of deep afterslip identified in previous models is still present.

We studied a period of 250 days since the main shock and focused on events with $M_w \geq 2.0$ for Parkfield and $M_w \geq 4.0$ for Tohoku. In order to restrict the parameter estimation to a time period in which the catalog is complete, we skipped a time window following the main shock, when the completeness magnitude is above these values ($t_0 = 100$ s for Parkfield and $t_0 = 5$ days for Tohoku). We estimated a background rate of $r_0 = 0.22 \text{ d}^{-1}$ for Parkfield and $r_0 = 0.2 \text{ d}^{-1}$ for Tohoku (for the areas shown in Figures 1 and 2, the completeness magnitudes mentioned above, and a time period between the start of the catalog and the main shock). Based on the resolution of the slip models and on computational requirements, we used a resolution of 0.025° (horizontal), 1 km (vertical) for Parkfield and 0.1° (horizontal), 3 km (vertical) for Tohoku.

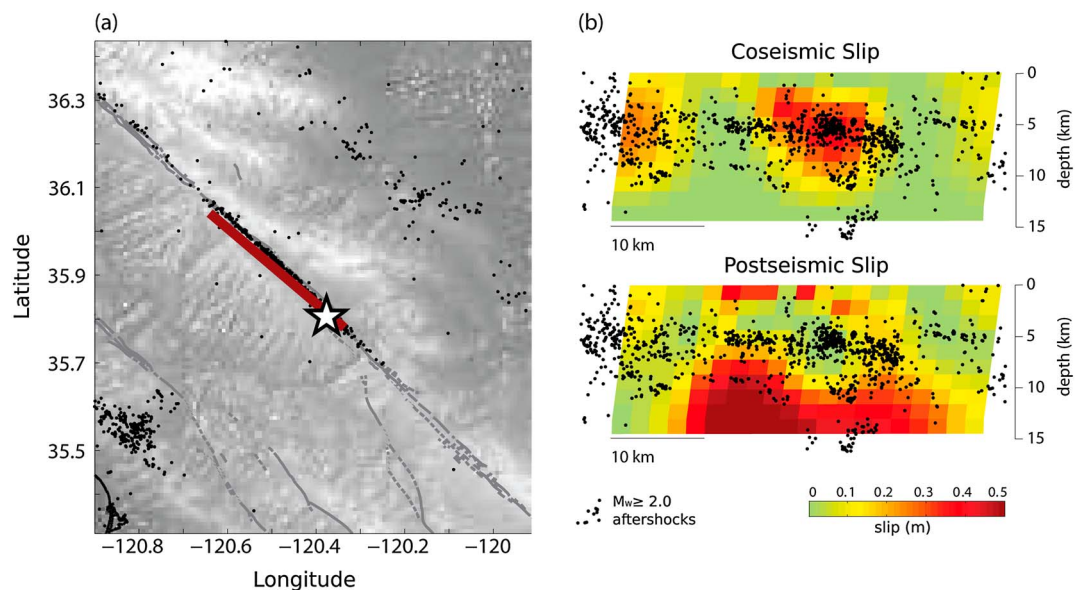


Figure 1. Map of the aftershock region of the September 2004 Parkfield earthquake. (a) Map view of $M_w \geq 2.0$ aftershocks in 250 days. (b) Coseismic and postseismic slip models from Figure 4 of *L. Wang et al. [2012]*, with aftershocks superimposed.

3. Results

As shown in Table 1, secondary triggering causes in both cases the most significant changes in log likelihood, with a probability gain of $I = 0.25$ for Parkfield and $I = 0.72$ for Tohoku; on the other hand, the inclusion of afterslip has an opposite effect on model performance for Parkfield and for Tohoku ($I = 0.10$ and $I = -0.41$, respectively). In section 1 of Text S1 in the supporting information, we estimate the significance of these values by comparing them with the internal variability of each forecast due to the Monte Carlo sampling of receiver fault orientations. Information gain differences are significant for all models in the case of Tohoku; for Parkfield, we find that the improvement in performance due to afterslip is small between

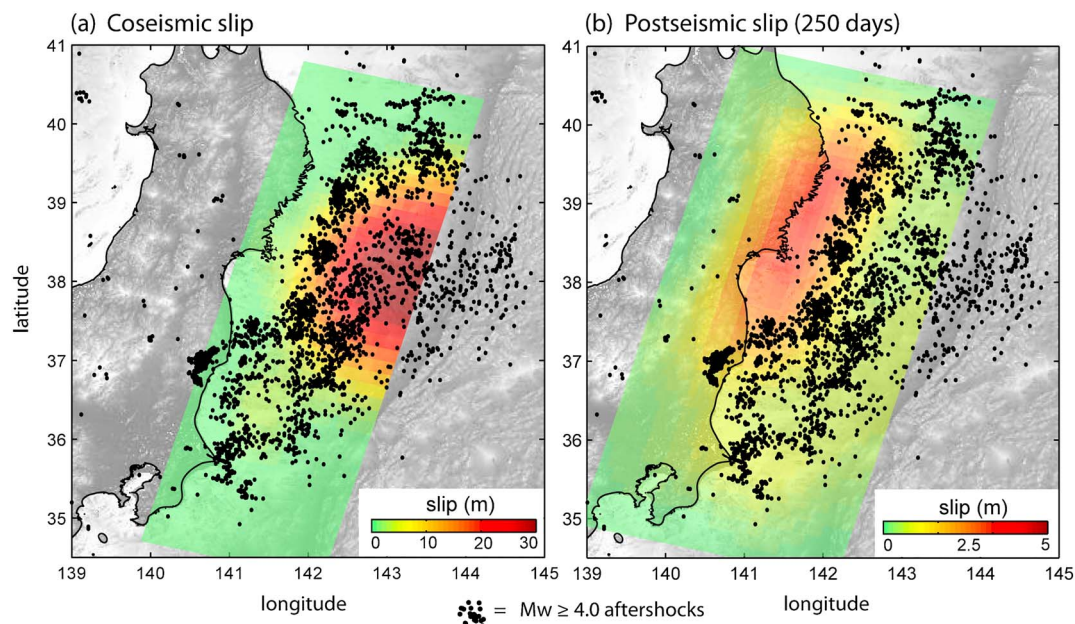


Figure 2. Map of the aftershock region of the March 2011 Tohoku earthquake. (a) Coseismic slip. (b) Cumulative afterslip after 250 days. Both slip models are from *Wang et al. [2013]*. Black dots are $M_w \geq 4.0$ aftershocks between 5 and 250 days.

Table 1. Rate-and-State Parameters and Model Performance for Parkfield and Tohoku

<i>Parkfield</i>						
Model	Afterslip	Secondary Triggering	$A\sigma$ (kPa)	t_a (Days)	N_{events} ($N_{\text{obs}} = 644$)	I^a
0	no	no	4.0	8000	447	0
1	yes	no	8.0	5000	515	0.10
2	no	yes	3.5	7000	619	0.25
3	yes	yes	5.5	5000	853	0.22
<i>Tohoku (Slip Model From Wang et al. [2013])</i>						
Model	Afterslip	Secondary Triggering	$A\sigma$ (kPa)	t_a (Days)	N_{events} ($N_{\text{obs}} = 1740$)	I
0	no	no	15.0	7000	1139	0.0
1	yes	no	19.0	8000	1651	-0.41
2	no	yes	15.0	7000	1445	0.72
3	yes	yes	19.0	8000	1923	0.54
<i>Tohoku (Slip Model From Perfettini and Avouac [2014])</i>						
Model	Afterslip	Secondary Triggering	$A\sigma$ (kPa)	t_a (Days)	N_{events} ($N_{\text{obs}} = 1740$)	I
0	no	no	40.0	16000	2179	0.0 (0.28 ^b)
1	yes	no	32.0	4000	2319	-0.08
2	no	yes	40.0	8000	2122	0.79
3	yes	yes	35.0	4000	2527	0.70

^a I is the information gain, i.e., the difference in log likelihood between each model and Model 0 divided by the total number of aftershocks.

^bInformation gain between Model 0 using the model from Perfettini and Avouac [2014] and Model 0 using the model from Wang et al. [2013].

models 0 and 1 and not significant between models 2 and 3. The ranking of the models is unchanged when using the coseismic and postseismic slip models of Perfettini and Avouac [2014]; however, we find variations in the optimal values of RS parameters, as well as the information gain and the total number of forecasted events. We notice that the change in performance due to the choice of the coseismic slip model ($I = 0.28$) is of the same order of the change due to the inclusion of afterslip, but smaller than the improvement achieved by modeling of secondary triggering.

For Parkfield we find that by redistributing slip along the main shock fault plane, afterslip modifies the location of the positive and negative lobes of the forecast, particularly to the southwest of the rupture plane (Figures 3a–3d). Secondary triggering, on the other hand, has almost no effect on the large-scale spatial distribution of seismicity. The model based on coseismic stresses (Figure 3e) predicts high seismicity in the surrounding of the rupture area, where stresses are highest, and low rates close to the area of maximum coseismic slip. The model which includes afterslip forecasts higher seismicity rates everywhere along the faults. The inclusion of aftershocks also leads to higher on-fault seismicity rates (also due to the lower value of $A\sigma$ for Model 2 than for Model 0) but does not change the spatial distribution significantly.

The first-order features of the forecast map for the Tohoku sequence agree with observed aftershocks (Figures 4a–4d); however, all models overestimate seismicity above the downdip edge of the fault plane and farther inland. This is probably caused by the use of a homogeneous background rate, since positive ΔCFS can generate large seismicity in areas which are aseismic, where the background rate is in reality close to zero. This behavior is accentuated by the inclusion of afterslip, which is concentrated at the downdip end of the fault plane. Models with afterslip also exhibit high seismicity rates at the downdip edge of the

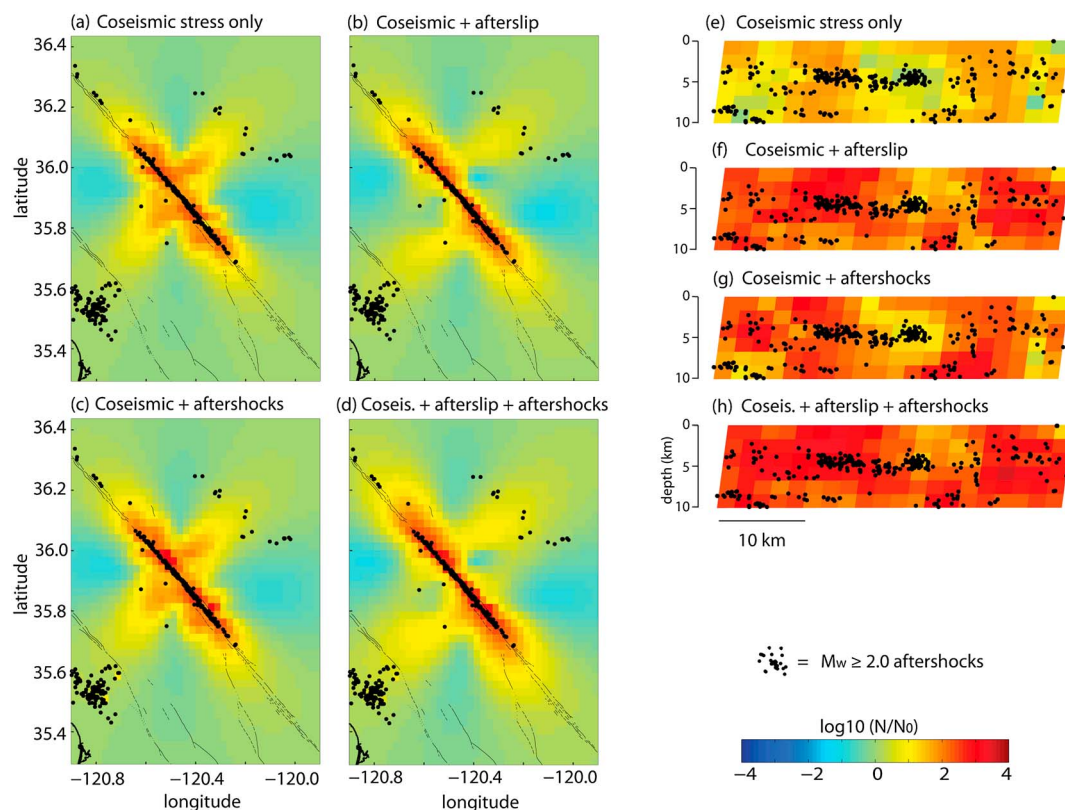


Figure 3. (a–d) Maps of forecasted seismicity in 250 days following Parkfield, summed over all depth layers. (e–h) Forecasted seismicity on the main shock rupture plane. The color indicates the number of forecasted events, divided by the background number (N_0), on a logarithmic scale. Black dots are the observed events; in Figures 3e–3h, only events within 5 km from the fault plane are shown. Figures 3a and 3e show model with coseismic stresses only; Figures 3b and 3f show model with coseismic stresses and afterslip; Figures 3c and 3g show model with coseismic stresses and secondary triggering; and Figures 3d and 3h show model with coseismic stresses, afterslip, and secondary triggering. RS parameters have been optimized for each case separately, and they differ between models (see Table 1).

fault: this is an artifact due to the geometry of the slip model, which is composed of three subfaults and presents a sharp change in dip at this depth. By calculating the log likelihood excluding the bottom 3 km, we verified that this feature does not affect the ranking of the models. Figures 4e–4h show the modeled and observed seismicity within 5 km of the slab. A qualitative inspection of Figure 4f suggests that aftershocks are located at the edges of the afterslip patch and not in the center: this is in agreement with the lower seismicity rates predicted in the afterslip area and consistent with triggering from the stress concentration at the edges of the area of afterslip. On the other hand, more careful observation indicates that some of the events occur within the area of predicted low seismicity; we return to the effect of afterslip on individual events in section 3.2 and discuss the uncertainties affecting the modeling of on-fault seismicity in section 4.

3.1. Temporal Distribution

To first degree, all models provide a good fit to the observed seismicity (Figures 5 and 6), but some discrepancies are present. The N test [Zecher *et al.*, 2010] can be used to assess whether models underestimated or overestimated seismicity rates. We performed this tests on individual 24 h forecasts: Table 2 summarizes the results. We find that daily forecasts pass the N tests on 92–97% of days for Parkfield and between 76 and 87% for Tohoku; all models tend to underestimate seismicity more often than they overestimate it, with the exception of Model 3 for Parkfield. In both cases, Model 0 is rejected most often, indicating that modeling of postseismic processes makes the models more successful. All models underestimate seismicity and fail the N test at the start: for Tohoku, Model 0 is rejected in the first 23 days and models 1–3 in the first 15 days. All models are rejected in the first day for Parkfield: an hourly N test performed on the first day of seismicity for Parkfield indicates that models 2 and 3 are rejected in the first 6 h, while models 0 and 1 are rejected in the first 12 and 14 h, respectively.

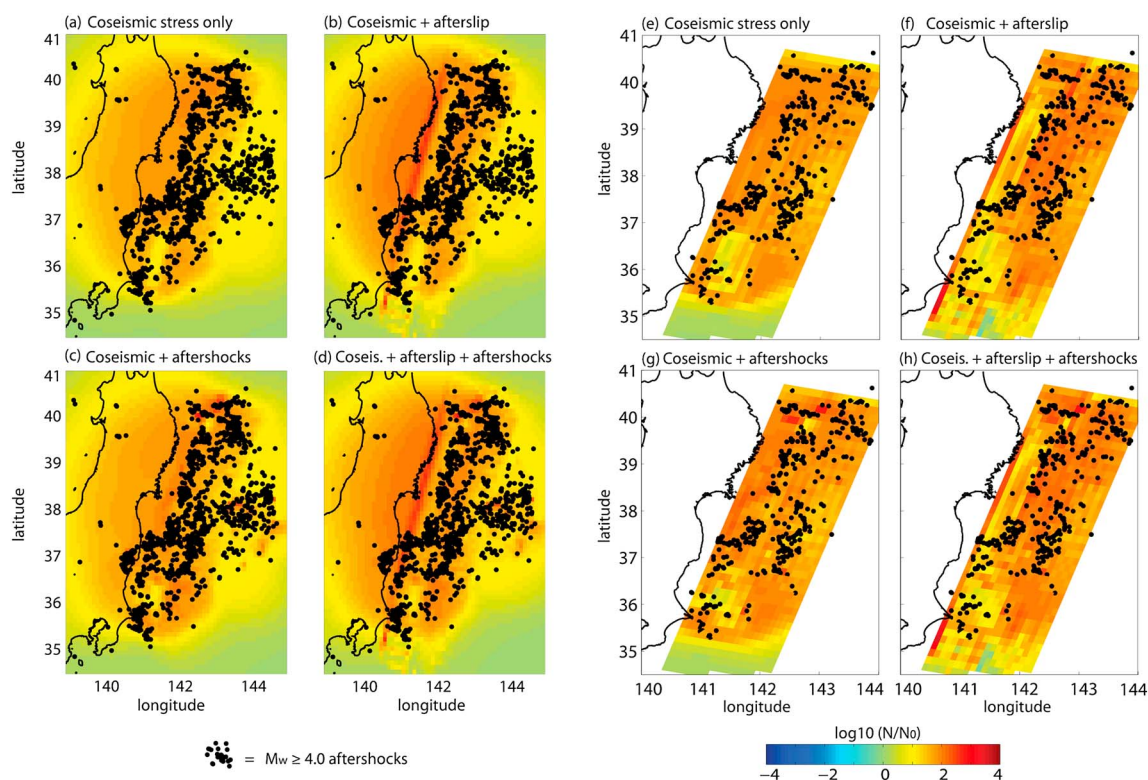


Figure 4. Maps of forecasted seismicity between 5 and 250 days following Tohoku, with RS parameters optimized separately for each model (see Table 1). Colors and figure numbers are the same as in Figure 3.

Afterslip leads to higher seismicity rates at later times and hence lower Omori p values: while the total number of events is better estimated (Table 1), the fit to the temporal decay worsens, as indicated by the Omori p values reported in Figures 5 and 6. We will return to a discussion of the misfit between the observed and modeled Omori decay in section 4.6.

3.2. Effect of Postseismic Stresses on Individual Events

In order to study the impact of postseismic stresses without the bias introduced by different constitutive parameters, we compare models with fixed rate-and-state parameters (for Tohoku, $A\sigma = 19$ kPa, $t_a = 8000$ days and for Parkfield, $A\sigma = 4$ kPa, $t_a = 8000$ days). To focus on the role of postseismic stresses on individual aftershocks, we compare the information gain of single events (equation (8)).

When considering afterslip after Parkfield, we find the largest positive information gains for a band of events at ~ 5 km depth, and for a cluster of deeper events (~ 10 km), respectively, updip and at the northwest edge of the afterslip area (Figure 7a). Negative I_{ev} are instead found for deeper earthquakes, within the afterslip patch. The values of I_{ev} do not appear to be time dependent (Figure 7c).

Also for Tohoku, most of the negative information gains come from events at the downdip end of the fault, in the vicinity of the maximum afterslip (Figure 8a), while an increase in probability is observed for events farther southwest, on the side of a high afterslip region. The I_{ev} values in Figure 8b suggest that on-fault aftershocks are not, on average, encouraged by afterslip; a clear temporal trend is not visible in Figure 8c.

The overall information gain is dominated by on-fault events, not only because they are more numerous but also because they experience the most dramatic changes, being closer to the slip. However, off-fault seismicity is important to understand from the hazard point of view; and since stress calculations are more reliable in the far field, several Coulomb-based seismicity studies exclude the near-fault region [King *et al.*, 2004; Toda *et al.*, 2012]. A cluster of events at ~ 35 – 50 km above the fault exhibits positive information gains ($I_{ev} > 0$ for 81% of the events; red points in Figure 8b) and an average probability gain of 1.17. These 187 events are mostly shallow (4–12 km), normal faulting earthquakes occurring in the vicinity of Fukushima (latitude $\sim 37^\circ$ N, longitude ~ 140.5 – 141° E), documented by Imanishi *et al.* [2012] and Kato *et al.* [2011]. They

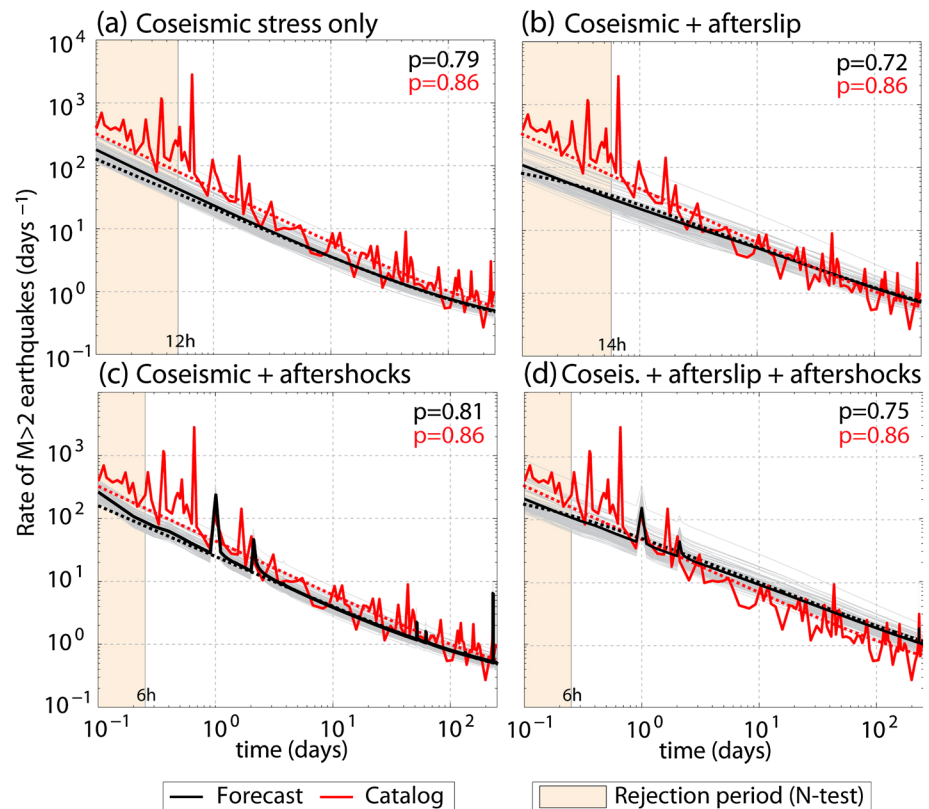


Figure 5. Temporal evolution of seismicity following Parkfield. Black lines: forecasted seismicity rates; red lines: observed rates. Each grey line represents seismicity resolved on a different receiver fault from the catalog of past focal planes, and the forecast is given by their average (details on the choice of receiver planes can be found in Cattania *et al.* [2014]). Dotted lines indicate the Omori fit obtained using log likelihood maximization (for the catalog) or a least squares fit (for the model forecasts), and the corresponding Omori p values are given. The shaded areas indicated time periods during which the forecasts are rejected based on a hourly N test (quantile score δ_1 at a 0.1 significance level).

start 30 days after the main shock and include one of the strongest aftershocks, the $M_w = 7.1$ Fukushima earthquake on 11 April; when the contribution from afterslip is accounted for, the seismicity rate at the location and time of this event increases by 37%.

Figures 7d–7f and 8d–8f indicate that secondary triggering leads to both positive and negative I_{ev} . Negative probability gains can be explained by two factors: first, aftershocks for which a synthetic slip model is used may produce stress shadows and second, models with secondary triggering forecast a larger number of events so that the integral term in equation (8) gives a negative contribution. For Parkfield most of the positive probability gains are found at early times and close distances to the fault (Figures 7e and 7f): since most of the aftershocks are aligned along a plane, they are likely to be triggered by previous events which generate $\Delta CFS > 0$ around their rupture area. For Tohoku, $I_{ev} > 0$ are found both in the near field and in the far field (in the overriding plate and in the outer rise; Figure 8e).

4. Discussion and Further Analysis

In both case studies, we find an improvement in model performance when considering secondary triggering. The effect of afterslip is more subtle and different between Parkfield and Tohoku: we will now discuss the limitations of our models, as well as testing the robustness of our result and their validity in a more general context.

4.1. Secondary Triggering

Modeling stresses from aftershocks is particularly challenging, since slip distributions or even focal planes are not always known. In fact, Meier *et al.* [2014] found that including ΔCFS from aftershocks decreases the predictive power of the Coulomb hypothesis, and Segou and Parsons [2014] found a negligible improvement

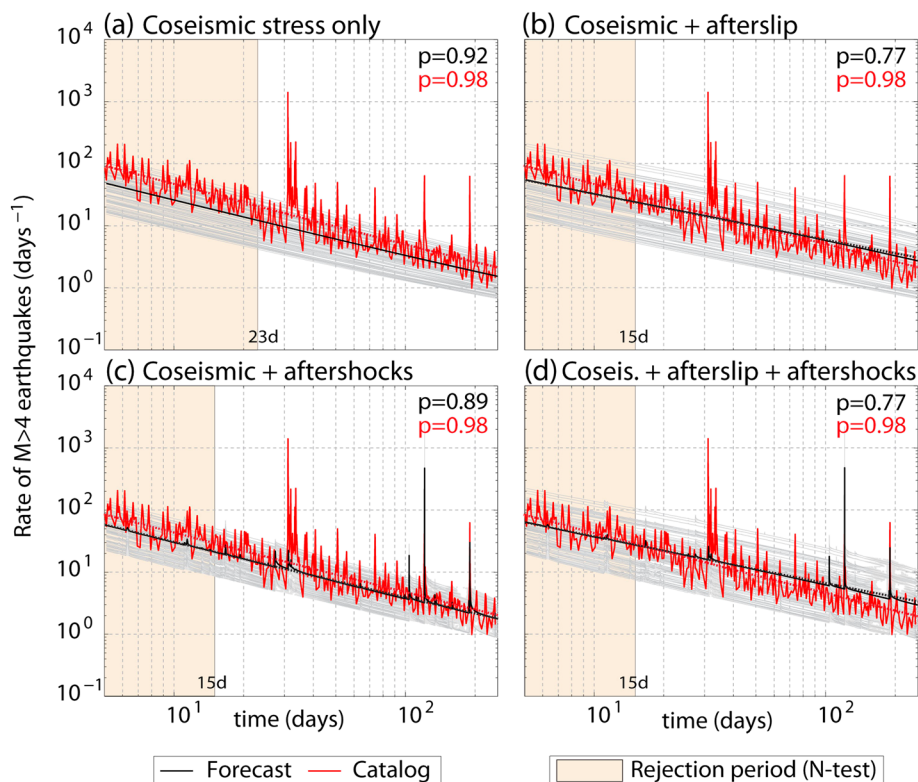


Figure 6. Temporal evolution of seismicity following Tohoku. Line colors are the same as in Figure 5.

in predictability. The difference between these results and the improvement in performance in our models may be due to the fact that for most of the events, we assumed an isotropic stress field instead of the full stress field from the focal mechanism. The full stress field is highly sensitive to uncertainties due to the assumption of a uniform slip model and nodal planes uncertainties. Indeed, we find, in agreement with Meier et al. [2014], that negative I_{ev} are in some cases associated with aftershocks with known focal mechanisms, for which we calculated a full anisotropic stress field. Due to the uncertainties involved in stress

calculations, the use of an isotropic stress field seems preferable from a forecasting perspective, and while not realistic from a physical point of view, this approach is in some way similar to the methods used by statistical models such as the epidemic-type aftershock sequences (ETAS) or smoothed seismicity models [Ogata, 1998; Helmstetter et al., 2007]. Another aspect to keep in mind for secondary triggering is the model resolution: for computational reasons, the grid size was in both cases significantly larger than the rupture length of the smallest aftershocks, and the results may be sensitive to position of a source within a grid cell. In order to extend the model to even smaller magnitude, a strategy based on adaptive mesh refinement may be appropriate.

Table 2. N Test Results Obtained With a Sliding Window of 24 h^a

Model	No. of Days With $\delta_1 < 0.05$	No. of Days With $\delta_2 < 0.05$	Percentage of Days Passing the N Test
<i>Parkfield</i>			
0	18	0	93%
1	7	0	97%
2	13	1	94%
3	2	9	96%
<i>Tohoku</i>			
0	59	0	76%
1	29	8	85%
2	44	1	82%
3	22	13	86%

^aThe second and third columns indicate the number of days rejected by the N test at a significance level of 0.1, respectively, due to underestimation and overestimation of the number of events; a daily forecast passes the N test if $\delta_1 \geq 0.05$ and $\delta_2 \geq 0.05$.

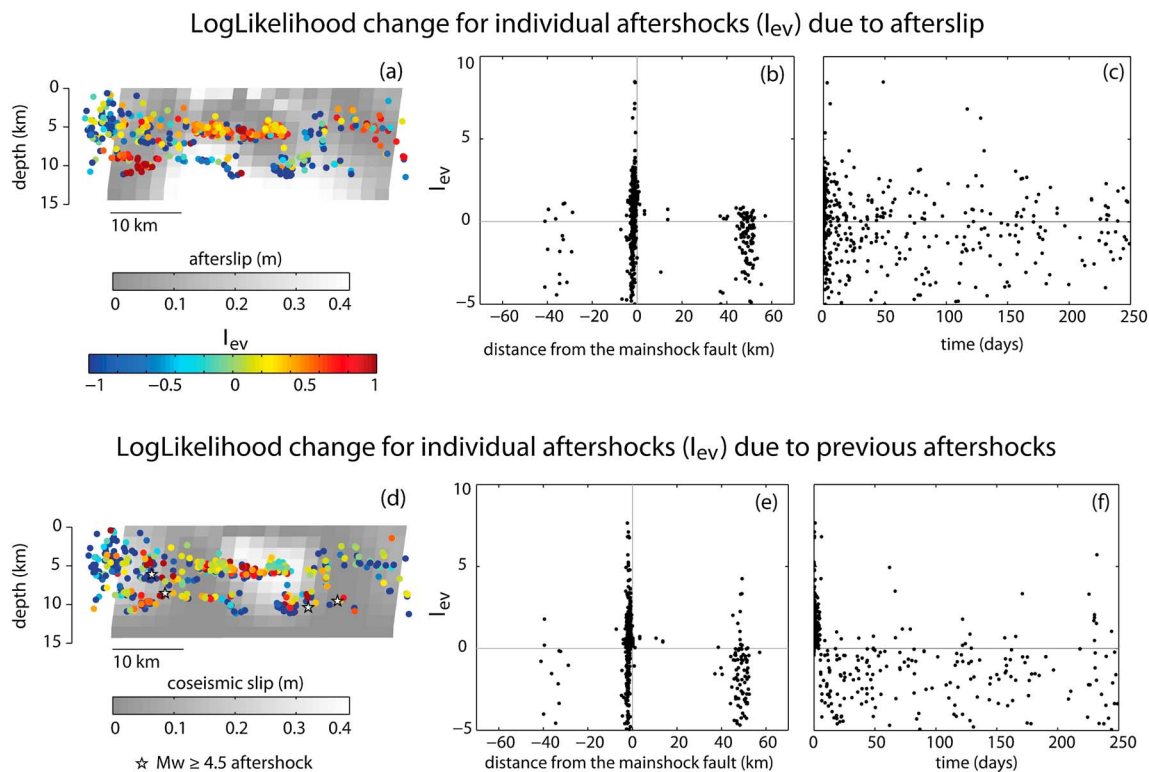


Figure 7. Change in log likelihood (I_{ev}) for individual events between Model 0 and models including postseismic stresses, with fixed RS parameters, for Parkfield. (a–c) Comparison to models including afterslip. Figure 7a shows aftershocks color coded by I_{ev} ; Figure 7b shows I_{ev} versus distance from the main shock fault plane; and Figure 7c shows I_{ev} versus time. (d–f) Comparison to models including secondary triggering.

4.2. Triggering of On-Fault Aftershocks by Coseismic Stresses Versus Afterslip

The inclusion of afterslip has a positive effect in model performance for Parkfield; in particular, reloading by afterslip improves the fit for events occurring within the rupture area, which experience negative coseismic stress. The overlap between aftershocks and the area of maximum coseismic slip, as well as the complementarity between coseismic and postseismic slip, is also observed with other published models [Johnson, 2006; Peng and Zhao, 2009; Langbein, 2006; Barbot et al., 2009]. This is in contrast with the observation that generally only few aftershocks occur in regions of high coseismic slip [Das and Henry, 2003]; the different behavior may be due to the fact that Parkfield was followed by an unusually large shallow afterslip, and reloading of the coseismic rupture area may have been more effective in this case than for the events analyzed by Das and Henry [2003].

Based on stress transfer, the areas of the fault which experience the largest stresses from coseismic and postseismic slip are those located close to the edge of the slip area; on the contrary, negative stresses are expected where the largest slip occurs. In order to model the stress generated by afterslip on neighboring aftershocks, the spatial error from the afterslip model and earthquake location should be small enough to clearly establish their relative position. However, modeling choices such as fault geometry and smoothing may give rise to large differences between published slip models, as discussed in the next section.

Even if a slip model was a perfect description of the slip distribution at long wavelengths, uncertainties would still exist on small scales because slip inversions have smoothness constraints due to limited information: therefore, inverted slip distributions are likely smoother than real ones. Various studies [Mai and Beroza, 2002] indicate that slip is fractal, and Marsan [2005] showed that the stress heterogeneity caused by fractal slip accounts for the observed seismicity in the vicinity of the fault; Lengliné and Marsan [2009] propose that small repeating earthquakes on or near the Parkfield rupture area are caused by a highly heterogeneous stress field.

Similar considerations also apply to the stress generated by afterslip. While afterslip is thought to have a smoother distribution than coseismic slip, a popular model of the subduction interface invokes

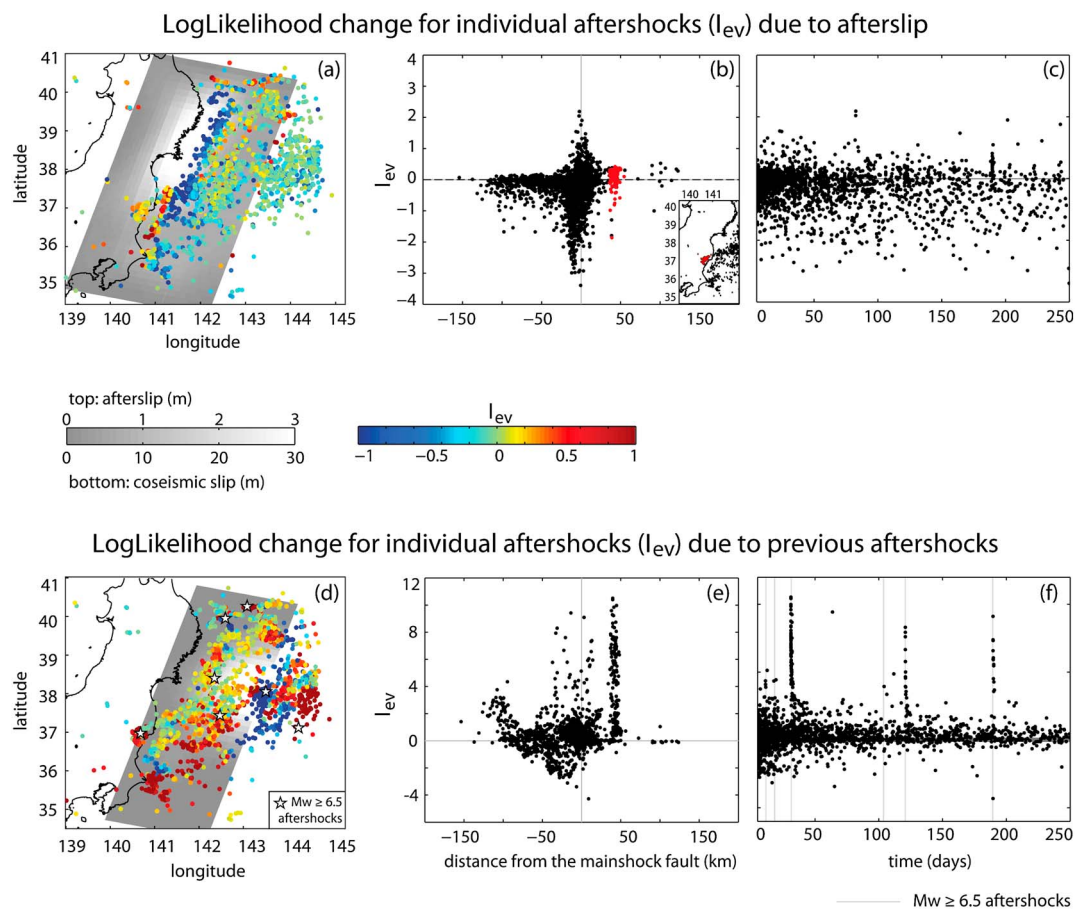


Figure 8. Effect of afterslip and secondary triggering on individual events for Tohoku. Subfigures correspond to those in Figure 7. Events in the vicinity of Fukushima (described in the main text) are highlighted in red, and they have an average probability gain $G = 1.17$. The slip models shown in the background are those from Wang et al. [2013].

heterogeneities in frictional properties [Lay and Kanamori, 1981]: isolated patches with velocity weakening friction (asperities) embedded in velocity strengthening material. In regions with a low density of asperities, earthquakes are decoupled and driven by the surrounding creep: the timing of repeating events lends support to this hypothesis [Schaff et al., 1998]. This mechanism cannot be captured by our model, since the seismic patches embedded in the afterslip regions are not resolved. This may account for the negative I_{ev} in Figures 7a and 8a.

4.3. Sensitivity to the Choice of Slip Model

Comparison of published afterslip models for the same main shock indicates that the details of the slip distribution are not well defined, and the exact location of the afterslip following Tohoku varies between models [Ozawa et al., 2011, 2012; Perfettini and Avouac, 2014]. As shown by Rietbrock et al. [2012] for the Maule earthquake, the discrepancies between slip models may be too large to draw clear conclusions about the relationship between slip and near-field aftershocks.

To address this issue, we calculate I_{ev} from afterslip for the slip model of Perfettini and Avouac [2014], with fixed RS parameters ($A\sigma = 19$ kPa, $t_a = 8000$ days). A comparison of Figure 9 with Figure 8 reveals that for events within 20 km from the fault interface, the effect of afterslip is very sensitive to the choice of slip model. In the Wang et al. [2013] model, most events updip of the afterslip area do not experience significant information gains. On the other hand, the model of Perfettini and Avouac [2014], in which most of the afterslip is shallow and partially overlaps with the coseismic slip, exhibits more dramatic information gains. The large variability of I_{ev} seen in Figure 9a can be attributed to the exact location of the events with respect to the megathrust and to their timing within the sequence (early events are less affected by afterslip and have I_{ev} close to 0; see section 4.5). The cluster of shallow seismicity in the vicinity of Fukushima, however,

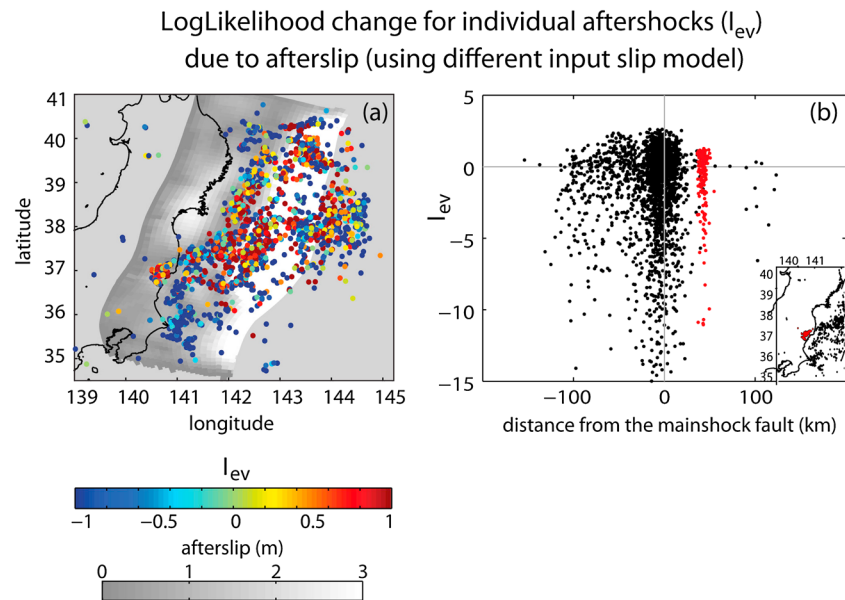


Figure 9. Effect of afterslip on individual events using the coseismic and afterslip model of *Perfettini and Avouac* [2014]. (a) Map view. (b) I_{ev} versus distance from the main shock fault plane. To allow direct comparison with Figure 8, distances from the fault are calculated with respect to the slip model of *Wang et al.* [2013].

presents more a consistent picture, since in both cases the probability of the events increases when considering afterslip. In spite of the negative I_{ev} seen in Figure 9b, the average probability gain of the cluster is 1.31; the seismicity rate at the time and location of the Fukushima event increases by 306%. While this value is larger than the one obtained from the slip models of *Wang et al.* [2013], in both cases we see a significant increase in probability, indicating that the contribution of afterslip to the triggering of this aftershock is not negligible.

4.4. Triggering of Shallow Crustal Events by Deep Afterslip in Subduction Zones

Our models indicate that afterslip plays an important role in triggering a cluster of shallow, normal fault aftershocks in the Fukushima region, and this result is robust with respect to input coseismic and postseismic slip models. This observation is particularly relevant from a hazard point of view, since these are intraplate events in the vicinity of urban centers, and they can be very destructive. The triggering of moderate size aftershocks in the hanging wall is a consistent feature of megathrust earthquakes: *Gomberg and Sherrod* [2014] showed that all $M_w \geq 8.6$ subduction main shocks since 1960 triggered crustal events of $M_w \geq 5.5$, usually at a distance of few fault lengths. Afterslip is also frequently observed following megathrust events [*Pritchard and Simons*, 2006]. In particular, afterslip downdip of the main shock rupture area is expected based on along-dip variations of the frictional properties of the fault: below the seismogenic depth, the fault is velocity strengthening and it responds to the coseismic stress changes by creep [*Hyndman et al.*, 1997; *Marone et al.*, 1991].

These considerations suggest that the enhancement of crustal seismicity by afterslip may be a common behavior following megathrust earthquakes. While an exhaustive study of several cases is beyond the scope of this work, we tested the effect of afterslip for the $M_w = 2010$ Maule (Chile) earthquake on 27 February 2010, which was followed by intense crustal seismicity in particular in the vicinity of Pichilemu, including a $M_w = 7.0$ and a $M_w = 6.8$ aftershocks on 11 March [*Ryder et al.*, 2012]. For this analysis, we used the slip models from *Bedford et al.* [2013] and events with $M_w \geq 2.0$ from the integrated plate boundary observatory chile (IPOC) catalog [*Lange et al.*, 2012], starting on 15 March. Similar to what was observed for Tohoku, we find that the average probability gain of events within 5 km of the Pichilemu aftershocks is 1.76. Positive I_{ev} are also found for earthquakes farther inland, at distances of more than 35 km above the fault (average probability gain = 1.52). The spread of I_{ev} for near-fault events is also similar to what was observed for Tohoku. It should be noted that unlike for Tohoku, for Maule the coseismic slip extends close to the crustal aftershocks near Pichilemu; in fact, *Ryder et al.* [2012] found that these events are consistent with static stress triggering

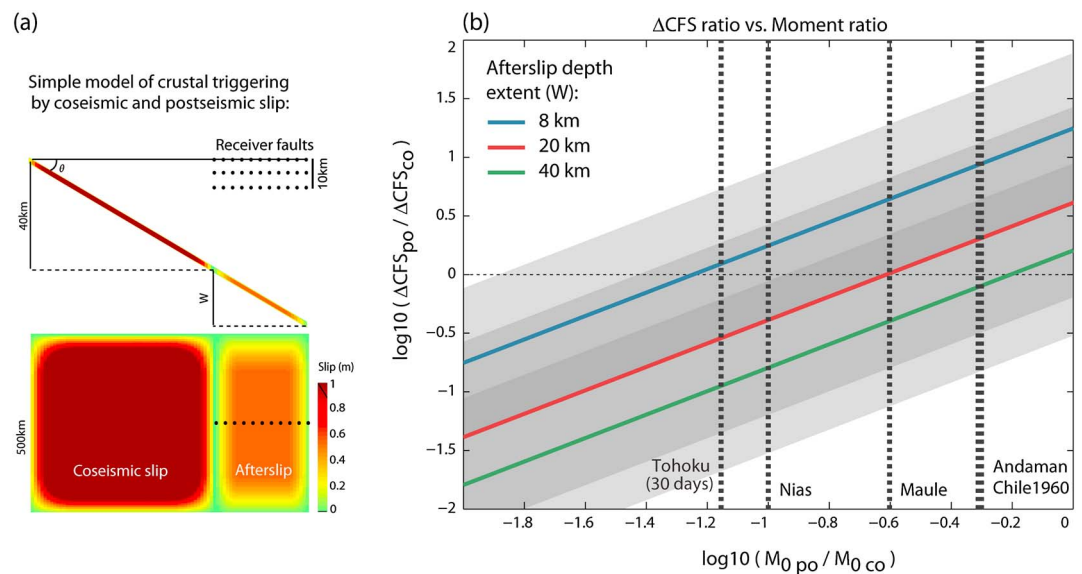


Figure 10. (a) Simplified model of crustal triggering on the hanging wall by coseismic slip and afterslip, for faults located above patches of high afterslip. Coulomb stresses are calculated on receiver faults at the locations indicated by the dots; at each location, a set of receiver faults are used, with strike close to trench parallel (strike = $0^\circ \pm 10^\circ$, $180^\circ \pm 10^\circ$) and dip between 60° and 90° . The dip of the slab is varied between 10° and 20° ; coseismic and postseismic slips are assumed to be uniform but tapered at the edges; a purely thrust mechanism is assumed, and the slip is varied to produce moment magnitudes between $M_w = 8.0$ and 9.0 (main shock) and $M_w = 6.5$ and 9.0 (afterslip). (b) Ratio between postseismic and coseismic stresses, as a function of seismic moment ratio. Each line corresponds to a different vertical extent of afterslip, corresponding to 20–100% of the coseismic rupture area. The grey area represents one standard deviation of the distributions obtained by varying the parameters described above. Vertical lines are the values of coseismic/postseismic moment ratio obtained from the literature (see supporting information, section 2).

from the main shock. Our results suggest that afterslip further enhances seismicity rates in an area which was already loaded by the coseismic stresses.

These findings may be surprising, since afterslip has a significantly lower amplitude than coseismic slip. A geometrical reason can be invoked to explain the results: for a shallow-dipping fault, deep slip may be located directly underneath the continent, closer to crustal normal faults than near-trench slip. To explore this geometrical effect, and to generalize our results to other subduction settings, we perform a Coulomb stress analysis for a simplified model of subduction, depicted in Figure 10a. Based on the analysis of *Ruff and Tichelaar* [1996], we assume coseismic slip extending down to a depth of 40 km, and afterslip on the same fault, directly downdip of the coseismic rupture; we vary the dip of the slab and the location and orientation of the receiver faults, located above the afterslip patch. For each of these different geometries, we calculate the ratio between postseismic and coseismic stresses as a function of the ratio of coseismic/postseismic moment (Figure 10b). Variations in the geometry of the receiver faults and slab dip introduce large variations in the stress ratio ($\Delta CFS_{po} / \Delta CFS_{co}$), but on average, postseismic stress changes exceed coseismic ones as long as the moment ratio is above ~ 0.6 . These values can directly be compared with seismic moment ratio of past great subduction earthquakes (given in section 2 of Text S1 in the supporting information). Based on the results from *Gomberg and Sherrod* [2014], we consider events larger than $M_w \geq 8.6$; for each of these events, visual comparison between the location of crustal aftershocks [*Gomberg and Sherrod*, 2014] and published afterslip models indicates that aftershocks have occurred close to the afterslip area, in agreement with the simple geometry in Figure 10a; the only exception is the 1964 Alaska earthquake (according to the slip model of *Suito and Freymueller* [2009]). Figure 10b indicates that following these megathrust earthquakes, afterslip-induced stresses on crustal faults were likely to be comparable to coseismic stresses and may therefore have played an important role in triggering crustal aftershocks.

4.5. Effect of Stress Evolution

In addition to the location of afterslip, the large information gain obtained for off-fault events may be enhanced by the time dependence introduced by the rate-and-state seismicity response. In order to isolate this aspect, we calculated the seismicity rate for a single stress step followed by afterslip with the same time

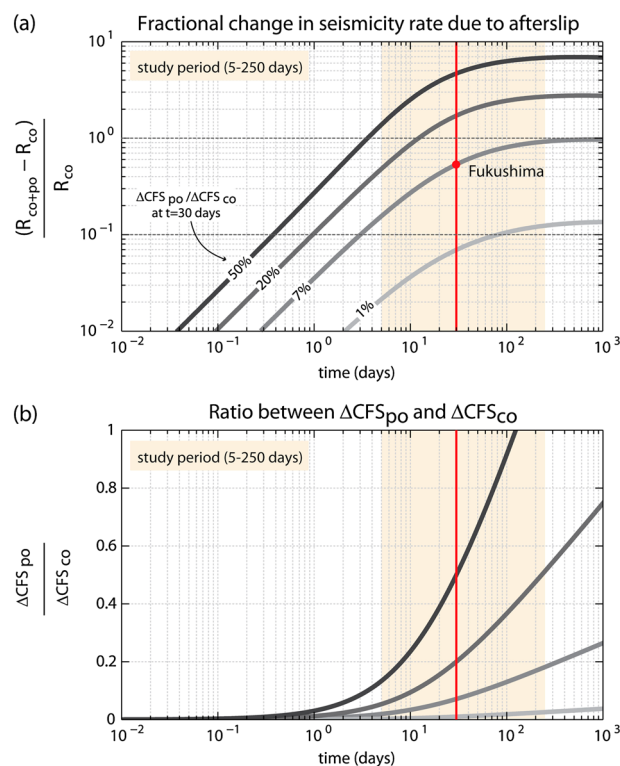


Figure 11. Effect of time-dependent stress changes on the seismicity rate, for a coseismic stress step of 0.32 MPa (the value calculated on the Fukushima fault); $A\sigma = 19$ kPa, $t_a = 18,000d$. The postseismic stress is given by $\Delta CFS_{po}(t) = \alpha \log(t/14.2 + 1)$, with α such that $\Delta CFS_{po}(30d)$ is between 1 and 50% of the coseismic stress. (a) Fractional change in seismicity rate due to the effect of afterslip. (b) Temporal evolution of ΔCFS_{po} normalized by coseismic stress, for the same curves as in Figure 11a. The red line indicates the time of the Fukushima aftershock.

4.6. Omori Decay

All the tested models exhibit a slower time decay than the catalog (Figures 5 and 6): the underestimation of the Omori p value can be due to several factors. In rate-and-state-based seismicity models, the time dependence of seismicity depends on the interplay between a variable stressing rate and the nucleation timescale imposed by the rate-and-state parameters. We tested a wide range of $A\sigma$, t_a to verify if a different choice of parameters would produce the observed temporal decay for Tohoku for a model with coseismic stresses and afterslip (Model 1): as shown in section 3 of Text S1 in the supporting information, we found similar p values (close to 0.75) for all the parameters tested. A second candidate are errors in the time-dependent input data, in particular for the models which include aftershocks as stress sources: the incompleteness of the catalog at early times will inevitably lead to underestimating early stresses over late ones, which may contribute to a slow decay in the modeled seismicity rate. We tested this possibility by creating a synthetic complete catalog, from which we then removed early events using the detection rate function of *Ogata and Katsura* [2006]; we found that in spite of the large difference in the total number of events used as sources (4885 and 3916), the difference in the time curves is negligible (less than 1%). A third explanation for the p value is the heterogeneity of the stress field. It has been shown [*Helmstetter and Shaw*, 2006] that stress heterogeneity leads to p values smaller than 1 and decreasing with increasing width of the stress distribution. In our model, stress heterogeneity comes from two aspects: the use of multiple receiver fault orientations and the spatial variability. The use of receiver fault orientations does not seem to be the most important aspect: the lines in Figures 5 and 6, representing individual receiver faults, are almost parallel to the average, indicating that the p value would not change significantly if stresses were resolved on a single receiver fault. The spatial heterogeneity of stresses may not have been overestimated in itself; however, by using a uniform background rate, we may have overestimated the importance of low stress areas, since the majority of the off-fault area is aseismic and would not contribute to the seismicity if

dependence as for the Tohoku model (section 2.4) and rate-and-state parameters as for Model 1 (Table 1); the amplitude of the postseismic stress is varied so that at $t = 30$ days the postseismic stress is between 1 and 50% of the coseismic stress. Figure 11 shows that during the study period, the fractional change in seismicity rate introduced by afterslip exceeds the ratio between postseismic and coseismic stresses by a factor of 8–10. For the Fukushima event, we find that this effect is more important than the geometrical aspect described above: the postseismic stress calculated directly on the focal plane of this aftershock is 7% of the coseismic stress; however, the enhancement in seismicity is 53%. It has been suggested that despite generating small stresses compared to coseismic slip, afterslip drives aftershock sequences [*Perfettini*, 2004]. While our models also include coseismic stresses, these results confirm that the time dependence of afterslip makes it a particularly effective triggering mechanism and that studies of earthquake triggering based purely on Coulomb stress analysis may severely underestimate the importance of afterslip at a given point in time.

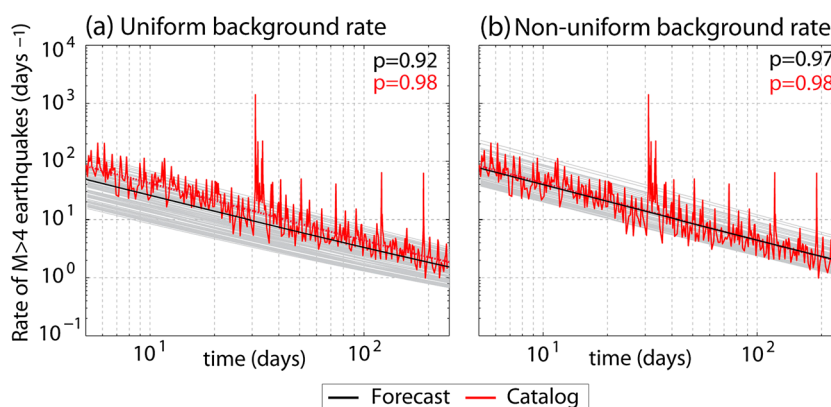


Figure 12. Comparison between seismicity decay obtained by assuming (a) uniform or (b) nonuniform background seismicity, for the Tohoku sequence. The nonuniform background seismicity model was calculated for the period between 1 January 2010 and the main shock, using the nearest neighbor algorithm [Helmstetter *et al.*, 2007], after declustering the catalog with the window method introduced by Gardner and Knopoff [1974]. We find that the increase in the Omori p value is a robust observation with respect to variations of the minimum smoothing distance, the cutoff magnitude, and the length of time window of the catalog.

a nonuniform background was used. We tested this aspect by running Model 0 for Tohoku with a nonuniform background rate, obtained from declustered, smoothed seismicity from 1 January 2010 until the main shock. Figure 12 indicates that using a nonuniform background leads to better temporal fit: the p value increases from $p = 0.92$ to $p = 0.97$, closer to the observed value of 0.98. Finally, we point out that in a space-time-dependent model, the effect of afterslip in the temporal evolution of seismicity depends not only on the slip rate but also on the spatial distribution of the afterslip: in particular, since areas with positive coseismic ΔCFS dominate early seismicity, the sign of the afterslip-induced ΔCFS in these regions may determine whether the net effect of afterslip is to accelerate or slow down seismicity. Appendix A shows a simple demonstration of how, only by changing the relative location of coseismic and postseismic stresses, the p value obtained from CRS models can significantly vary (in our example, between 0.85 and 1.65).

By using a space-independent CRS formulation, Savage [2010] obtained a good fit for the decay of aftershocks following Parkfield. While Figure 5 seems to contradict these results, we conclude that the sensitivity of a space-dependent model to the background seismicity and to the relative location of coseismic/postseismic stress changes makes it challenging to obtain reliable results on the time decay of seismicity.

4.7. Modeling Assumptions

In addition to the uncertainties related to the input data, several simplifications are made in our models. We focus on two sources of time-dependent stresses and neglected the impact of viscoelastic relaxation and poroelastic effects. Viscoelastic relaxation typically acts on a longer timescale than afterslip, and its contribution may be negligible in the time frame we consider [Diao *et al.*, 2014]. In contrast, poroelastic effects are expected on the same timescale as afterslip, but modeling them would require detailed assumptions on the poorly constrained value of the hydraulic diffusivities in the seismogenic volume.

The consideration of stress heterogeneities has a profound impact on CRS models. We take into account one source of stress variability, namely, the existence of multiple receiver fault orientations, by sampling from the catalog of previous focal planes: as described in Cattania *et al.* [2014], we considered to some extent the spatial variations in the distribution of focal planes. However, a more detailed consideration of spatial variability may be implemented, in particular by including information of the existing fault systems. Finally, the assumption of uniform background seismicity is an oversimplification, and as shown in section 4.6 it can significantly affect model behavior. While previous studies [Cocco *et al.*, 2010] indicate that using a nonuniform background leads to potentially unstable results, Bhloscaidh *et al.* [2014] found an improvement in the forecast ability of Coulomb-based models when considering spatial variations of background rate. Stable estimations of the background rate are therefore an important challenge for the future.

4.8. Relevance for Operational Earthquake Forecasting

Physics-based aftershock models typically perform less well than statistical models [Woessner *et al.*, 2011]. This is due to different reasons, including the large uncertainties in stress calculations and the difficulties in reproducing realistic stress heterogeneity. For our case studies, model performance improves significantly when secondary triggering is taken into account: this result may explain, to some extent, the poor performance of CRS models compared to statistical models which explicitly or implicitly include the effect of previous aftershocks, such as the ETAS models or smoothed seismicity models. We point out, however, that this study represents a best case scenario, since we used earthquake catalogs released months after the main shock, with a lower completeness magnitude and smaller errors than real-time data. Further testing, especially in a prospective setting, should be carried out to verify the generality of our findings and the potential gains for earthquake forecasting.

Our approach to including afterslip data is also not applicable to an operational forecasting setting, since afterslip models are currently not available in real time; moreover, including afterslip may not be beneficial in terms of model performance, as measured by log likelihood. On the other hand, the observation of crustal seismicity being favored by afterslip seems a robust feature of our model for the Tohoku sequence, and it may be a common feature following megathrust earthquakes. While detailed modeling of afterslip may not be feasible in real time, monitoring of crustal deformation may be used to directly estimate the stress increases, and hence the triggering potential, in these areas.

5. Conclusions

We performed a study on the role of postseismic stresses in triggering aftershocks, based on Coulomb stress transfer and the rate-and-state constitutive law of earthquake nucleation.

In terms of model performance, we find that stress redistribution by aftershocks plays a first-order role, in spite of the fact that aftershocks account for a small fraction of seismic moment compared to the main shock and afterslip. This result may explain, to some extent, the poor performance of physics-based seismicity models compared to statistical models which take into account secondary triggering [Woessner *et al.*, 2011].

The effect of afterslip on model performance is more difficult to assess. In the vicinity of the rupture plane, where slip model uncertainties are large and the relative location of afterslip and aftershocks is not well determined, robust conclusions on the role of afterslip to trigger aftershocks are difficult to draw, especially for Tohoku. For Parkfield, reloading by afterslip may explain the occurrence of aftershocks on the coseismic rupture area, a feature common to several coseismic slip models; however, this observation can also be explained by unresolved small-scale slip heterogeneity, and the relative role of the two factors remains

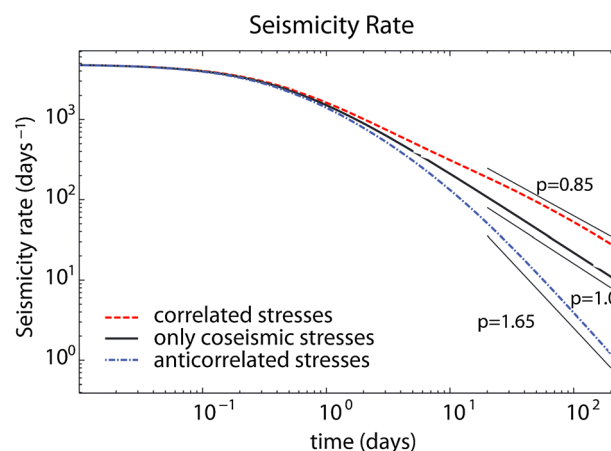


Figure A1. Temporal evolution of seismicity for the simple model described in the text. The black, red, and blue lines correspond to models without afterslip, with afterslip correlated to coseismic slip, and with afterslip anticorrelated with coseismic slip. The total coseismic and postseismic stresses are the same in all cases.

an open question. At distances farther than few tens of kilometers from the main shock fault, we find that afterslip generally enhances seismicity; in particular, crustal inland aftershocks in the Fukushima region following the Tohoku earthquake are promoted by afterslip. The enhancement of shallow seismicity in the hanging wall by afterslip seems to be a common feature of large subduction earthquakes: a simple model of afterslip following great megathrusts indicates that for typical seismic moment ratios, trench parallel crustal fault systems experience higher stresses from afterslip than would be expected based on the seismic moment. Given the hazard posed by onshore aftershocks, the topic deserves further study: in particular, we suggest that a more detailed

description of the fault orientation in these areas, as well as consideration of viscoelastic and poroelastic response, could give more insight on the seismic activation of these regions. Finally, we show that afterslip time dependence is an important aspect to consider: in the study period, the effect of postseismic stresses on seismicity rate is amplified by the rate-and-state response of the model, and the triggering potential of afterslip would be severely underestimated by a time-independent Coulomb stress analysis.

Appendix A: Dependence of the P Value on the Relative Location of Coseismic and Postseismic Stresses

As explained in the main text, large uncertainties exist in coseismic and postseismic models, and their relative location can vary across models. To test how these uncertainties may affect the temporal evolution of seismicity, we use a simple model composed of two regions, experiencing coseismic stresses of ± 0.1 MPa. Postseismic stresses with a logarithmic time dependence ($\tau \propto \log(1 + t/t^*)$, $t^* = 14$ days) are superimposed to each region, reaching a value of ± 0.05 MPa in 250 days. We computed seismicity evolution using equation (B21) from Dieterich [1994] and compared a case in which the sign of coseismic/postseismic stresses is the same in each region and a case in which they are instead anticorrelated. Figure A1 shows that the two cases result in very different Omori p values (1.65 and 0.85, respectively), indicating that the spatial distribution of slip may have a profound role in determining the temporal evolution predicted by CRS models.

Acknowledgments

We thank E. Rivalta for comments on this manuscript and H. Perfettini, J. P. Avouac, and J. Bedford for providing their slip models. This research was carried out in the framework of REAKT project (Strategies and Tools for Real-Time Earthquake Risk Reduction) founded by the European Community via the Seventh Framework Program for Research (FP7), contract 282862. C.C. is a member of the Helmholtz graduate research school GeoSim. We are grateful to the Japan Meteorological Agency for providing the catalog data used in this study. The data used for this study are available from the following websites: ANSS catalog (determined by Northern California Seismic Network, USGS, Menlo Park, and Berkeley Seismological Laboratory, University of California, Berkeley), <http://quake.geo.berkeley.edu/anss/>; focal mechanisms catalog for Southern California, <http://www.data.scec.org/research-tools/alt-2011-yang-hauksson-shearer.html>; and focal mechanisms catalog for Japan (F-net moment-tensor focal mechanisms solutions), <http://www.fnet.bosai.go.jp/event/search.php>.

References

- Barbot, S., Y. Fialko, and Y. Bock (2009), Postseismic deformation due to the M_w 6.0 2004 Parkfield earthquake: Stress-driven creep on a fault with spatially variable rate-and-state friction parameters, *J. Geophys. Res.*, *114*, B07405, doi:10.1029/2008JB005748.
- Barrientos, S. E., and S. N. Ward (1990), The 1960 Chile earthquake: Inversion for slip distribution from surface deformation, *Geophys. J. Int.*, *103*(3), 589–598, doi:10.1111/j.1365-246X.1990.tb05673.x.
- Bedford, J., et al. (2013), A high-resolution, time-variable afterslip model for the 2010 Maule $M_w = 8.8$, Chile megathrust earthquake, *Earth Planet. Sci. Lett.*, *383*, 26–36, doi:10.1016/j.epsl.2013.09.020.
- Benioff, H. (1951), Earthquakes and rock creep, *Bull. Seism. Soc. Am.*, *41*, 31–62.
- Bhloscaidh, M. N., J. McCloskey, and C. J. Bean (2014), Response of the San Jacinto Fault Zone to static stress changes from the 1992 Landers earthquake, *J. Geophys. Res. Solid Earth*, *119*, 8914–8935, doi:10.1002/2014JB011164.
- Cattania, C., S. Hainzl, L. Wang, F. Roth, and B. Enescu (2014), Propagation of Coulomb stress uncertainties in physics-based aftershock models, *J. Geophys. Res. Solid Earth*, *119*, 7846–7864, doi:10.1002/2014JB011183.
- Chen, K. H., R. Bürgmann, and R. M. M. Nadeau (2013), Do earthquakes talk to each other? Triggering and interaction of repeating sequences at Parkfield, *J. Geophys. Res. Solid Earth*, *118*, 165–182, doi:10.1029/2012JB009486.
- Cocco, M., and J. R. Rice (2002), Pore pressure and poroelasticity effects in Coulomb stress analysis of earthquake interactions, *J. Geophys. Res.*, *107*(B2), 2030, doi:10.1029/2000JB000138.
- Cocco, M., S. Hainzl, F. Catalli, B. Enescu, A. M. Lombardi, and J. Woessner (2010), Sensitivity study of forecasted aftershock seismicity based on Coulomb stress calculation and rate- and state-dependent frictional response, *J. Geophys. Res.*, *115*, B05307, doi:10.1029/2009JB006838.
- Das, S., and C. Henry (2003), Spatial relation between main earthquake slip and its aftershock distribution, *Rev. Geophys.*, *41*(3), 1013–2003, doi:10.1029/2002RG000119.
- Diao, F., X. Xiong, R. Wang, Y. Zheng, T. R. Walter, H. Weng, and J. Li (2014), Overlapping post-seismic deformation processes: Afterslip and viscoelastic relaxation following the 2011 M_w 9.0 Tohoku (Japan) earthquake, *Geophys. J. Int.*, *196*(1), 218–229, doi:10.1093/gji/ggt376.
- Dieterich, J. (1994), A constitutive law for rate of earthquake its application to earthquake clustering, *J. Geophys. Res.*, *99*, 2601–2618.
- Gardner, J., and L. Knopoff (1974), Is the sequence of earthquakes in southern California, with aftershocks removed, Poissonian, *Bull. Seism. Soc. Am.*, *64*(5), 1363–1367.
- Gomberg, J., and B. Sherrod (2014), Crustal earthquake triggering by modern great earthquakes on subduction zone thrusts, *J. Geophys. Res. Solid Earth*, *119*, 1235–1250, doi:10.1002/2012JB009826.
- Gualandi, A., E. Serpelloni, and M. E. Belardinelli (2014), Space-time evolution of crustal deformation related to the M_w 6.3, 2009 L'Aquila earthquake (central Italy) from principal component analysis inversion of GPS position time-series, *Geophys. J. Int.*, *197*(1), 174–191, doi:10.1093/gji/ggt522.
- Hainzl, S., B. Enescu, M. Cocco, J. Woessner, F. Catalli, R. Wang, and F. Roth (2009), Aftershock modeling based on uncertain stress calculations, *J. Geophys. Res.*, *114*, B05309, doi:10.1029/2008JB006011.
- Hainzl, S., S. Steacy, and D. Marsan (2010), *Seismicity Models Based on Coulomb Stress Calculations*, Community Online Resource for Statistical Seismicity Analysis, 10 November 2010 Version: 1.0, doi:10.5078/corssa-32035809, [Available at http://www.corssa.org/articles/themev/hainzl_et_al].
- Helmstetter, A., and B. E. Shaw (2006), Relation between stress heterogeneity and aftershock rate in the rate-and-state model, *J. Geophys. Res.*, *111*, B07304, doi:10.1029/2005JB004077.
- Helmstetter, A., and B. E. Shaw (2009), Afterslip and aftershocks in the rate-and-state friction law, *J. Geophys. Res.*, *114*, B01308, doi:10.1029/2007JB005077.
- Helmstetter, A., Y. Y. Kagan, and D. D. Jackson (2007), *High-resolution Time-independent Grid-based Forecast for $M \geq 5$ Earthquakes in California*, vol. 78, pp. 78–86.
- Hsu, Y.-J., P. Segall, S.-B. Yu, L.-C. Kuo, and C. A. Williams (2007), Temporal and spatial variations of post-seismic deformation following the 1999 Chi-Chi, Taiwan earthquake, *Geophys. J. Int.*, *169*(2), 367–379, doi:10.1111/j.1365-246X.2006.03310.x.

- Hyndman, R. D., M. Yamano, and D. A. Oleskevich (1997), The seismogenic zone of subduction thrust faults, *Island Arc*, *6*, 244–260.
- Imanishi, K., R. Ando, and Y. Kuwahara (2012), Unusual shallow normal-faulting earthquake sequence in compressional northeast Japan activated after the 2011 off the Pacific coast of Tohoku earthquake, *Geophys. Res. Lett.*, *39*, L09306, doi:10.1029/2012GL051491.
- Johnson, K. M. (2006), Frictional properties on the San Andreas Fault near Parkfield, California, inferred from models of afterslip following the 2004 earthquake, *Bull. Seism. Soc. Am.*, *96*(4B), S321–S338, doi:10.1785/0120050808.
- Kagan, Y. (2004), Short-term properties of earthquake catalogs and models of earthquake source, *Bull. Seism. Soc. Am.*, *94*(4), 1207–1228.
- Kato, A., S. Sakai, and K. Obara (2011), A normal-faulting seismic sequence triggered by the 2011 off the Pacific coast of Tohoku earthquake: Wholesale stress regime changes in the upper plate, *Earth Planets Space*, *63*, 745–748, doi:10.5047/eps.2011.06.014.
- King, G. C. P., R. S. Stein, and J. Lin (2004), Static stress changes and the triggering of earthquakes, *Bull. Seism. Soc. Am.*, *84*(3), 935–953.
- Langbein, J. (2006), Coseismic and initial postseismic deformation from the 2004 Parkfield, California, earthquake, observed by Global Positioning System, electronic distance meter, creepmeters, and borehole strainmeters, *Bull. Seism. Soc. Am.*, *96*(4B), S304–S320, doi:10.1785/0120050823.
- Lange, D., et al. (2012), Aftershock seismicity of the 27 February 2010 M_w 8.8 Maule earthquake rupture zone, *Earth Planet. Sci. Lett.*, *317*–*318*, 413–425, doi:10.1016/j.epsl.2011.11.034.
- Lay, T., and H. Kanamori (1981), An asperity model of large earthquake sequences, in *Earthquake Prediction: An International Review, Maurice Ewing Ser.*, vol. 4, edited by D. Simpson and P. Richards, pp. 579–592, AGU, Washington, D. C.
- Lengliné, O., and D. Marsan (2009), Inferring the coseismic and postseismic stress changes caused by the 2004 M_w = 6 Parkfield earthquake from variations of recurrence times of microearthquakes, *J. Geophys. Res.*, *114*, B10303, doi:10.1029/2008JB006118.
- Linker, M. F., and J. H. Dieterich (1992), Effects of variable normal stress on rock friction: Observations and constitutive equations, *J. Geophys. Res.*, *97*(92), 4923–4940.
- Mai, P. M., and G. C. Beroza (2002), A spatial random field model to characterize complexity in earthquake slip, *J. Geophys. Res.*, *107*, 2308, doi:10.1029/2001JB000588.
- Marone, C., C. H. Scholz, and R. Bilham (1991), On the mechanics of earthquake afterslip, *J. Geophys. Res.*, *96*(91), 8441–8452.
- Marsan, D. (2005), The role of small earthquakes in redistributing crustal elastic stress, *Geophys. J. Int.*, *163*(1), 141–151, doi:10.1111/j.1365-246X.2005.02700.x.
- Meier, M., M. J. Werner, J. Woessner, and S. Wiemer (2014), A search for evidence of secondary static stress triggering during the 1992 M_w 7.3 Landers, California, earthquake sequence, *J. Geophys. Res. Solid Earth*, *119*, 3354–3370, doi:10.1002/2013JB010385.
- Nur, A., and J. R. Booker (1972), Aftershocks caused by pore fluid flow?, *Science*, *175*(4024), 885–887, doi:10.1126/science.175.4024.885.
- Ogata, Y. (1998), Space-time point-process models for earthquake occurrences, *Ann. Inst. Stat. Math.*, *50*(2), 379–402.
- Ogata, Y., and K. Katsura (2006), Immediate and updated forecasting of aftershock hazard, *Geophys. Res. Lett.*, *33*, L10305, doi:10.1029/2006GL025888.
- Okada, Y. (1992), Internal deformation due to shear and tensile faults in a half-space, *Bull. Seism. Soc. Am.*, *82*(2), 1018–1040.
- Ozawa, S., T. Nishimura, H. Suito, T. Kobayashi, M. Tobita, and T. Imakiire (2011), Coseismic and postseismic slip of the 2011 magnitude-9 Tohoku-Oki earthquake, *Nature*, *475*, 373–376, doi:10.1038/nature10227.
- Ozawa, S., T. Nishimura, H. Munekane, H. Suito, T. Kobayashi, M. Tobita, and T. Imakiire (2012), Preceding, coseismic, and postseismic slips of the 2011 Tohoku earthquake, Japan, *J. Geophys. Res.*, *117*, B07404, doi:10.1029/2011JB009120.
- Peng, Z., and P. Zhao (2009), Migration of early aftershocks following the 2004 Parkfield earthquake, *Nat. Geosci.*, *2*(12), 877–881, doi:10.1038/ngeo697.
- Perfettini, H. (2004), Postseismic relaxation driven by brittle creep: A possible mechanism to reconcile geodetic measurements and the decay rate of aftershocks, application to the Chi-Chi earthquake, Taiwan, *J. Geophys. Res.*, *109*, B02304, doi:10.1029/2003JB002488.
- Perfettini, H., and J. P. Avouac (2014), The seismic cycle in the area of the 2011 M_w 9.0 Tohoku-Oki earthquake, *J. Geophys. Res. Solid Earth*, *119*, 4469–4515, doi:10.1002/2013JB010697.
- Pritchard, M. E., and M. Simons (2006), An aseismic slip pulse in northern Chile and along-strike variations in seismogenic behavior, *J. Geophys. Res.*, *111*, B08405, doi:10.1029/2006JB004258.
- Rietbrock, a., I. Ryder, G. Hayes, C. Haberland, D. Comte, S. Roecker, and H. Lyon-Caen (2012), Aftershock seismicity of the 2010 Maule M_w = 8.8, Chile, earthquake: Correlation between co-seismic slip models and aftershock distribution?, *Geophys. Res. Lett.*, *39*, L08310, doi:10.1029/2012GL051308.
- Ruff, L., and B. Tichelaar (1996), What controls the seismogenic plate interface in subduction zones?, in *Subduction Top to Bottom, Geophys. Monogr. Ser.*, vol. 96, edited by G. E. Bebout et al., pp. 105–111, AGU, Washington, D. C., doi:10.1029/GM096p0105.
- Ryder, I., A. Rietbrock, K. Nelson, R. Bürgmann, M. Floyd, A. Socquet, C. Vigny, and D. Carrizo (2012), Large extensional aftershocks in the continental forearc triggered by the 2010 Maule earthquake, Chile, *Geophys. J. Int.*, *188*(3), 879–890, doi:10.1111/j.1365-246X.2011.05321.x.
- Savage, J. C. (2010), Calculation of aftershock accumulation from observed postseismic deformation: M6 2004 Parkfield, California, earthquake, *Geophys. Res. Lett.*, *37*, L13302, doi:10.1029/2010GL042872.
- Savage, J. C., J. L. Svarc, and S.-B. Yu (2007), Postseismic relaxation and aftershocks, *J. Geophys. Res.*, *112*, B06406, doi:10.1029/2006JB004584.
- Schaff, D. P., G. C. Beroza, and B. E. Shaw (1998), Postseismic response of repeating aftershocks time-dependent recurrence, *Geophys. Res. Lett.*, *25*(24), 4549–4552.
- Segou, M., and T. Parsons (2014), The stress shadow problem in physics-based aftershock forecasting: Does incorporation of secondary stress changes help?, *Geophys. Res. Lett.*, *41*, 3810–3817, doi:10.1002/2013GL058744.
- Strader, A., and D. D. Jackson (2014), Near-prospective test of Coulomb stress triggering, *J. Geophys. Res. Solid Earth*, *119*, 3064–3075, doi:10.1002/2013JB010780.
- Suito, H., and J. T. Freymueller (2009), A viscoelastic and afterslip postseismic deformation model for the 1964 Alaska earthquake, *J. Geophys. Res.*, *114*, B11404, doi:10.1029/2008JB005954.
- Toda, S., R. S. Stein, G. C. Beroza, and D. Marsan (2012), Aftershocks halted by static stress shadows, *Nat. Geosci.*, *5*(6), 410–413, doi:10.1038/ngeo1465.
- Wang, K., Y. Hu, and J. He (2012), Deformation cycles of subduction earthquakes in a viscoelastic Earth, *Nature*, *484*(7394), 327–32, doi:10.1038/nature11032.
- Wang, L., S. Hainzl, G. Zöller, and M. Holschneider (2012), Stress- and aftershock-constrained joint inversions for coseismic and postseismic slip applied to the 2004 M6.0 Parkfield earthquake, *J. Geophys. Res.*, *117*, B07406, doi:10.1029/2011JB009017.
- Wang, L., J. Liu, J. Zhao, and J. Zhao (2013), Co- and post-seismic modeling of the 2011 M_w 9 Tohoku-oki earthquake, and its impact on China mainland, *Earthquake (in Chinese)*, *33*(4), 238–246.

- Wells, D. W., and K. J. Coppersmith (1994), New empirical relationships among magnitude, rupture length, rupture width, rupture area, and surface displacement, *Bull. Seismol. Soc. Am.*, *84*(4), 974–1002.
- Woessner, J., S. Hainzl, W. Marzocchi, M. J. Werner, A. M. Lombardi, F. Catalli, B. Enescu, M. Cocco, M. C. Gerstenberger, and S. Wiemer (2011), A retrospective comparative forecast test on the 1992 Landers sequence, *J. Geophys. Res.*, *116*, B05305, doi:10.1029/2010JB007846.
- Woessner, J., S. Jónsson, H. Sudhaus, and C. Baumann (2012), Reliability of Coulomb stress changes inferred from correlated uncertainties of finite-fault source models, *J. Geophys. Res.*, *117*, B07303, doi:10.1029/2011JB009121.
- Zakharova, O., S. Hainzl, and C. Bach (2013), Seismic moment ratio of aftershocks with respect to main shocks, *J. Geophys. Res. Solid Earth*, *118*, 5856–5864, doi:10.1002/2013JB010191.
- Zechar, J. D., M. C. Gerstenberger, and D. A. Rhoades (2010), Likelihood-based tests for evaluating space-rate-magnitude earthquake forecasts, *Bull. Seismol. Soc. Am.*, *100*(3), 1184–1195, doi:10.1785/0120090192.
- Zhuang, J., D. Harte, M. J. Werner, S. Hainzl, and S. Zhou (2012), *Basic models of Seismicity: Temporal Models*, Community Online Resource for Statistical Seismicity Analysis, doi:10.5078/corssa-79905851, [Available at http://www.corssa.org/articles/themev/zhuang_et_al_a]